3D Rigorous Simulation of Mask Induced Polarization

Xiuhong Wei*[a], H.P.Urbach[b], Arthur Wachters[b], Yuri Aksenov[c]

[a] Optical Research Group, Department of Imaging Science and Technology,
Delft University of Technology, P.O. Box 5046, 2600 GA Delft, The Netherlands;
[b]Philips Research Laboratory,Professor Holstlaan 4, 5656 AA Eindhoven, The Netherlands;
[c]Philips Research Leuven, Kapeldreef 75, B-3001 Leuven,Belgium

ABSTRACT

The polarization induced by the mask is studied by using a 3D rigorous model, which solves Maxwell equations using the finite element method. The aerial image depends strongly on the change of polarization induced by the materials, thickness of the layer and pitch of the periodic masks.

Keywords: high NA, polarization, mask topography, rigorous simulation, 3D modeling

1. INTRODUCTION

The polarization induced by the mask has become one of the considerations in high NA lithography. We have applied a general electromagnetic 3D-model to study polarization effects of the mask.[1] The 3D model that we made uses the finite element method to solve Maxwell's equations. It can be applied to many other configurations rather than those studied in this paper, for example to an isolated scatterer in a multilayer, a 1D grating, and to a bi-grating. The materials may be inhomogeneous and/or anisotropic and they can be dielectrics or conductors. For completeness, also linear magnetic materials are allowed. Because the finite element method is applied, many different topographies can be handled. Furthermore, the incident field is unrestricted, it can, for example, be a plane wave of any wavelength with arbitrary polarization and arbitrary oblique angle of incidence or it can be a focused spot. Thus, the model is also applicable to investigate an influence of topography in resist.

The model is applied to the rigorous simulation of the effects of 1D/2D contact holes with bias and scattering bars. After explaining the general mathematical and numerical properties of the 3D model, we will consider the application to high NA lithographical systems, with 193-nm (ArF) immersion technology. The plane waves leaving the illumination system, which could be TE (electric field is perpendicular to the plane of incidence) or TM (electric field is in the plane of incidence), are diffracted by the 3D geometry of the mask. The masks considered are a binary chrome on-glass mask, an attenuated phase-shifting mask (APSM) of Silicon Nitride (Si_3N_4) and an advanced photomask with optical proximity correction (OPC). The calculated aerial image shows the influence of the materials of which the mask consists, of the type of mask, the thickness of the mask and the pitch of the mask. The results show that polarization effects induced by the mask depend strongly on the type of mask, the materials of which it is made and the angles of incidence of the incident plane waves. In comparison, the mask topography has less influence, although its effect is not negligible.

2. MATHEMATICAL MODEL

2.1. Scattering Problem

The imaging of two-dimensional periodic patterns of contact holes will be addressed in this paper, therefore we will only consider configurations which are periodic w.r.t. two coordinates x and y (Fig.1), with periods p_x and p_y in the x and y direction, respectively. We assume that all the materials are isotropic and not magnetic, i.e., the relative electric permittivity $\epsilon_r(\mathbf{r})$ is a periodic complex function and the relative magnetic permeability $\mu \equiv 1$

Further author information: (Send correspondence to X.Wei)
X. Wei: E-mail: wei@natlab.research.philips.com, Telephone: +31 (0)40 27 43 796
H. P. Urbach: E-mail: h.p.urbach@philips.com, Telephone: +31 (0)40 27 43 864
A. J. H. Wachters: E-mail: arthur.wachters@philips.com
Y. Aksenov: E-mail:aksenov@imec.be

Optical Microlithography XVIII, edited by Bruce W. Smith,
Proceedings of SPIE Vol. 5754 (SPIE, Bellingham, WA, 2005)
0277-786X/05/$15 · doi: 10.1117/12.597732

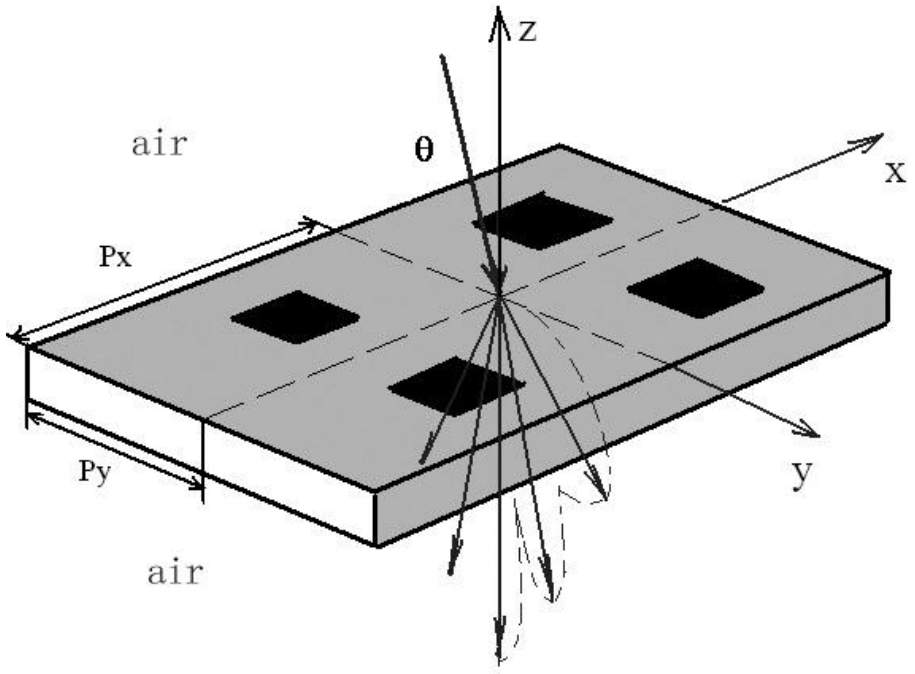

Figure 1. Configuration of the periodic scattering problem.

everywhere. We choose $a < b$ such that $z < a$ and $z > b$ both are half spaces (consisting of air in application discussed here). The illumination of the mask is by a perpendicular or oblique plane wave coming from the upper half space $z > b$ which is in air. The incident electric field $\mathbf{E}^i(\mathbf{r})$ is given by:

$$\mathbf{E}^i(\mathbf{r}) = \mathbf{A} \exp[i(\mathbf{kr} - \omega t)], \tag{1}$$

where $\mathbf{k} = (k_x, k_y, -k_z)$ is the incident wave vector with $k_z = \sqrt{\omega^2 \epsilon_0 \mu_0 - k_x^2 - k_y^2}$, with ω the frequency of the light and $\mathbf{A}$ the complex amplitude which satisfies $\mathbf{A} \cdot \mathbf{k} = 0$. Since the electromagnetic field is always time-harmonic, the factor $\exp(-i\omega t)$ will be omitted from now on. The total complex electric field $\mathbf{E}(\mathbf{r})$ satisfied near and inside the mask the vector Helmholtz equation:

$$\omega^2 \epsilon_0 \mu_0 \epsilon_r(\mathbf{r}) \mathbf{E}(\mathbf{r}) - \boldsymbol{\nabla} \times \boldsymbol{\nabla} \times \mathbf{E}(\mathbf{r}) = \mathbf{0}, \tag{2}$$

with boundary condition:

$$\text{Periodicity in the sense:} \quad \mathbf{E}(x + m_x p_x, y + m_y p_y, z) = \exp\left[i\left(k_x m_x p_x + k_y m_y p_y\right)\right] \mathbf{E}(x, y, z), \quad \text{for all integer } m_x, m_y, \tag{3}$$

and radiation conditions:

$$\mathbf{E}(\mathbf{r}) - \mathbf{E}^i(\mathbf{r}) \text{ consists in } z > b \text{ of plane waves that are propagating or are evanescent in the positive z-direction,} \tag{4}$$

$$\mathbf{E}(\mathbf{r}) \text{ consists in } z < a \text{ of plane waves that are propagating or are evanescent in the negative z-direction.} \tag{5}$$

Now we define the scattered field $\mathbf{E}^s(\mathbf{r})$, as the field due to the non-trivial scatterers only, i.e., the field that is scattered by all scatterers except for infinite planes that are parallel to the x- and y-axis. The field scattered by only the multilayer (if present) is called $\mathbf{E}^0$. For example, when the configuration consists of a periodic pattern

of holes in a multilayer, then the field scattered by the multilayer in the absence of the holes is called $\mathbf{E}^0$ and the scattered field due to the holes only is then defined by:

$$\mathbf{E}^s = \mathbf{E} - \mathbf{E}^0. \tag{6}$$

The field $\mathbf{E}^0$, $\mathbf{H}^0$ scattered by the multilayer can of course be determined analytically and hence will be assumed to be known. Then (2) implies that the scattered field satisfies:

$$\omega^2 \epsilon_0 \mu_0 \epsilon_r \mathbf{E}^s - \boldsymbol{\nabla} \times \boldsymbol{\nabla} \times \mathbf{E}^s = -\omega^2 \epsilon_0 \mu_0 (\epsilon_r - \tilde{\epsilon}_r) \mathbf{E}^0. \tag{7}$$

where $\tilde{\epsilon}_r(z)$ is piecewise constant relative electric permittivity of the multilayer. Furthermore, $\mathbf{E}^s$ satisfies (3) and the outgoing radiation conditions (4) and (5).

2.2. Reformulation of the Boundary Value Problem

It is more convenient to introduce periodic fields. Let us therefore write:

$$\begin{aligned} \mathbf{E}^0(\mathbf{r}) &= \mathbf{U}^0(\mathbf{r}) \exp[i(k_x x + k_y y)], \\ \mathbf{E}^s(\mathbf{r}) &= \mathbf{U}^s(\mathbf{r}) \exp[i(k_x x + k_y y)]. \end{aligned} \tag{8}$$

Then $\mathbf{U}^0$ and $\mathbf{U}^s$ are (p_x, p_y)-periodic and $\mathbf{U}^s$ satisfies

$$\omega^2 \epsilon_0 \mu_0 \epsilon_r(\mathbf{r}) \mathbf{U}^s(\mathbf{r}) - \boldsymbol{\nabla}_{k_x,k_y} \times \boldsymbol{\nabla}_{k_x,k_y} \times \mathbf{U}^s(\mathbf{r}) = -\omega^2 \epsilon_0 \mu_0 (\epsilon_r - \tilde{\epsilon}_r) \mathbf{U}^0, \tag{9}$$

where

$$\boldsymbol{\nabla}_{k_x,k_y} = \left(ik_x + \frac{\partial}{\partial x}, ik_y + \frac{\partial}{\partial y}, \frac{\partial}{\partial z} \right)^T. \tag{10}$$

The mathematical formulation of the boundary conditions (4) and (5), lead to double Fourier series which in general are slowly converging and hence are rather difficult to implement in an efficient way. Therefore instead of using these double Fourier series, we use the so-called PML (Perfectly matched layer, which was introduced by Berenger[2]). First we introduce a computational box Ω defined by

$$\Omega = (0, p_x) \times (0, p_y) \times (a, b) \tag{11}$$

Hence Ω contains one period in the x- and y-direction and is such that above and below Ω there are homogeneous

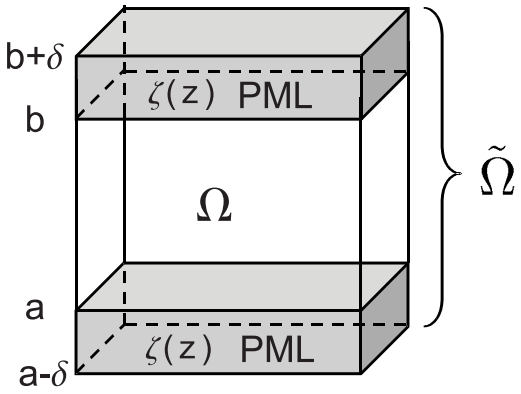

Figure 2. Example of a PML for a bi-grating. Since the problem is periodic w.r.t x and y, only two blocks of PML are needed.

half spaces. Next we extend Ω in the z-direction and the differential equation for the scattered field is modified in the additional region. This is done in such a way that:

1. No reflections are generated at the interface between Ω and the extension.

2. The field that penetrates the extension, which is the so called PML, is strongly absorbed there.

The extended region $\tilde{\Omega}$ is defined by:

$$\tilde{\Omega} = (0, p_x) \times (0, p_y) \times (a - \delta, b - \delta) \tag{12}$$

for some $\delta > 0$ (Fig.2). The PML $\tilde{\Omega} \backslash \Omega$ is filled with material with permittivity identical to that of the adjacent material in Ω. Furthermore, inside the PML the differential operator $\boldsymbol{\nabla}_{k_x,k_y}$ that occurs in (9) is replaced by

$$\boldsymbol{\nabla}^{\zeta}_{k_x,k_y} = \left(ik_x + \frac{\partial}{\partial x}, \, ik_y + \frac{\partial}{\partial x_y}, \, \frac{\partial}{\zeta \partial x_z} \right)^T, \tag{13}$$

where $\zeta(z)$ is a complex valued function with values in the first quadrant of complex plane and with

$$\zeta(z) = 1, \text{ for points on } \partial\Omega. \tag{14}$$

Hence inside the PML we have:

$$\omega^2 \epsilon_0 \mu_0 \epsilon_r(\mathbf{r}) \mathbf{U}^s(\mathbf{r}) - \boldsymbol{\nabla}^{\zeta}_{k_x,k_y} \times \boldsymbol{\nabla}^{\zeta}_{k_x,k_y} \times \mathbf{U}^s(\mathbf{r}) = -\omega^2 \epsilon_0 \mu_0 (\epsilon_r - \tilde{\epsilon}_r) \mathbf{U}^0, \text{ in } \tilde{\Omega} \backslash \Omega \tag{15}$$

The complex valued ζ cause a strong damping in the PML so that we can safely assume that $\mathbf{U}^s$ vanishes on the outer boundary $z = a - \delta$ and $z = b + \delta$. Furthermore, it can be shown that at the interface between the computational box Ω and the PML no reflection occurs. Hence we end up with the following boundary value problem on the extended region $\tilde{\Omega}$:

$$\omega^2 \epsilon_0 \mu_0 \epsilon_r(\mathbf{r}) \mathbf{U}^s(\mathbf{r}) - \boldsymbol{\nabla}^{\zeta}_{k_x,k_y} \times \boldsymbol{\nabla}^{\zeta}_{k_x,k_y} \times \mathbf{U}^s(\mathbf{r}) = -\omega^2 \epsilon_0 \mu_0 (\epsilon_r - \tilde{\epsilon}_r) \mathbf{U}^0, \text{ in } \tilde{\Omega} \tag{16}$$

$$\mathbf{U}^s(\mathbf{r}) \text{ is } (p_x, p_y) - \text{periodic}, \tag{17}$$

$$\mathbf{U}^s(\mathbf{r}) = 0 \left(\text{ or } \mathbf{n} \times \boldsymbol{\nabla}^{\zeta}_{k_x,k_y} \times \mathbf{U}^s(\mathbf{r}) = 0 \right) \text{ on the outer boundary of the PML .} \tag{18}$$

2.3. Finite Element Method

Let $\mathbf{V}$ be a periodic vector field that is sufficiently smooth. Take the scalar product of $\mathbf{V}$ with (16) and partial integrate using the boundary conditions. Then we obtain

$$\begin{aligned} \iiint_{\tilde{\Omega}} \left[\omega^2 \epsilon_0 \mu_0 \epsilon_r(\mathbf{r}) \, \mathbf{U}^s \cdot \mathbf{V} - \left(\boldsymbol{\nabla}^{\zeta}_{k_x,k_y} \times \mathbf{U}^s \right) \cdot \boldsymbol{\nabla}^{\zeta}_{k_x,k_y} \times \mathbf{V} \right] \mathrm{d}\mathbf{r} \\ = - \iiint_{\bar{\Omega}} \omega^2 \epsilon_0 \mu_0 (\epsilon_r - \tilde{\epsilon}_r) \mathbf{U}^0 \cdot \mathbf{V} \, d\mathbf{r}. \end{aligned} \tag{19}$$

From this variational formulation the finite element matrix is obtained as follows. First the region $\tilde{\Omega}$ is discretized by a mesh consisting of tetrahedra. On this mesh we consider piecewise linear vector fields $\phi_\nu(\mathbf{r})$ whose tangential component along an edge ν of the mesh is unity and which vanish on all tetrahedra of which ν is not an edge. Then we interpolate the scattered field as follows:

$$\mathbf{U}^s(\mathbf{r}) \quad = \quad \sum_{\nu \in \bar{\Omega} \cup \partial\bar{\Omega}} u^s_\nu \, \phi_\nu(\mathbf{r}), \text{ for } \mathbf{r} \in \tilde{\Omega}, \tag{20}$$

where u^s_ν is the mean value of the tangential component of $\mathbf{U}^s$ along edge ν. By substituting (20) into (19) and by choosing $\mathbf{V} = \phi_\nu(\mathbf{r})$ for all edges ν, we obtain the linear system:

$$\sum_\nu A_{\mu\nu} u^s_\nu = w_\mu, \tag{21}$$

where

$$A_{\mu\nu} = \iiint_{\tilde{\Omega}} \left[\omega^2 \epsilon_0 \mu_0 \epsilon_r(\mathbf{r})\, \phi_\nu \cdot \phi_\mu - \left(\boldsymbol{\nabla}^{\zeta}_{k_x,k_y} \times \phi_\nu \right) \cdot \boldsymbol{\nabla}^{\zeta}_{k_x,k_y} \times \phi_\mu \right] \zeta \, \mathrm{d}\mathbf{r}, \quad \text{for all edges } \nu, \mu \in \tilde{\Omega}, \tag{22}$$

and

$$w_\mu = \iiint_{\Omega} -\omega^2 \epsilon_0 \mu_0 (\epsilon_r - \tilde{\epsilon}_r) \mathbf{E}^0 \cdot \phi_\mu \, \mathrm{d}\mathbf{r} \tag{23}$$

Since the matrix is very large, it must be solved by an iterative solver. Because the matrix is indefinite, preconditioning is a highly nontrivial problem.

3. RESULTS

By using methods described in the previous sections, simulations were done to investigate some polarization effects induced by the mask. We consider two types of masks. The first one is the binary Chromium mask with three kinds of mask shapes of which top view and cross section are shown in Fig. 3. In all cases the Chromium is situated under a poly layer that is 0.5mm thick, the periods p_x and p_y are the same and the geometry is symmetric with respect to interchanging x and y. In Fig. 4 the second type of mask is show. It is the Si_3N_4 attenuated phase shifting mask (APSM). For this mask the periods p_x and p_y are again the same, the shape of the Si_3N_4 is square and the substrate is again a 0.5mm thick layer of poly.

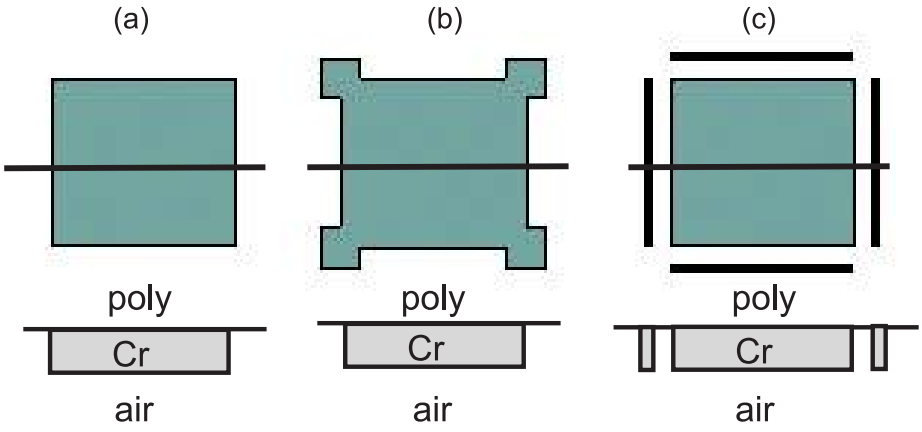

Figure 3. One period of the binary Chromium masks. The chromium is either square (a), or square with serifs (b) or square with bars (c). The horizontal lines through the middle are cut planes to which the cross sections shown correspond.

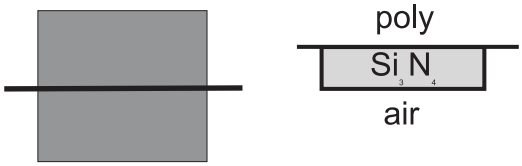

Figure 4. One period of the Attenuated phase shifting mask (APSM) consisting of Si_3N_4. The square dark region is Si_3N_4 at bottom of poly.

The refractive index n and absorption coefficient k of the different materials at the wavelength of $\lambda = 193$nm are listed in Table 1.

The mask is illuminated by a plane wave whose plane of incidence is the (x, z)-plane. This implies that for a TE polarized incident plane wave, the incident electric field is parallel to the y-axis, whereas for a TM polarized

Table 1. Material data of the masks.

Material	chromium	Si_3N_4	Poly
n	0.86	2.45	1.56
k	1.65	0.3	0

incident plane wave, the incident electric field is parallel to the y-axis, whereas for a TM polarized incident wave the incident magnetic field is parallel to the y-axis. The angle between the incident wave vector and the optical (z-) axis is either chosen to be 0^o (on-axis) or is chosen as 11 degrees in poly (off-axis). For the on-axis case there obviously is no difference between the TE and TM case when x and y are interchanged.

Let T_{TE} and T_{TM} be the transmissivity in the transmitted zero order when the incident plane is TE and TM polarized, respectively. The degree of polarization is defined by

$$DoP = \frac{T_{TE} - T_{TM}}{T_{TE} + T_{TM}}. \tag{24}$$

We first vary the pitch p_x=p_y of the masks. In Fig. 5 the transmitted intensity shown as are as function of the pitch for the binary Chromium mask of Fig. 3(a). The thickness of the Chromium is 70nm and the incident plane wave is perpendicular (on-axis). It is seen that the transmission sharply drops near p_x=$p_y = 1.5\lambda$.

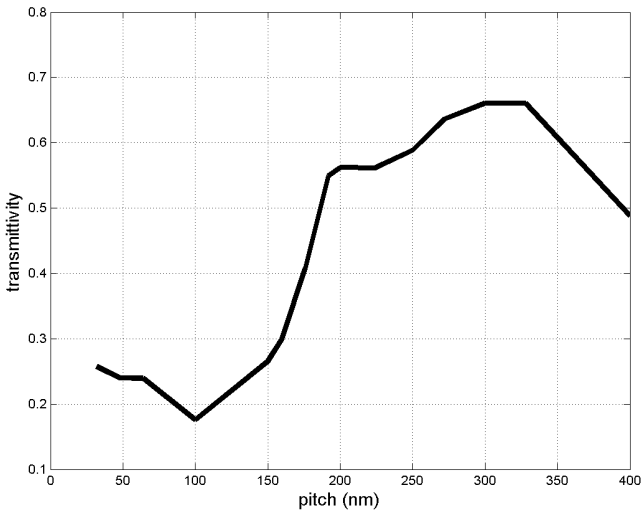

Figure 5. Transmittivity for binary Chromium mask with thickness 70nm. The illumination is on-axis. 0th order results for λ =193nm.

In Fig. 6 the degree of polarization is shown when the illumination is off-axis. For pitch smaller than 300nm the transmission for TM is larger than for TE, whereas for pitch larger than 1.5λ the inverse happens.

In Fig. 7 the illumination is again on-axis. In this case we vary the thickness of the chromium from 30 to 70nm, whereas the pitch is kept at $p_x = p_y$ = 400nm. The transmission of 0th order at first increases with thickness but slowly decreases above a thickness of 60nm.

Next we consider the APSM shown on Fig. 4. In Fig. 8 the degree of polarization is shown as function of the pitch for off-axis illumination. The thickness of the Si_3N_4 layer is 70nm. The 0th order DoP reaches a minimum at approximately $p_x = p_y = 250nm$, and increases gradually from $p_x = p_y = 300nm$. Just as the Chromium case the transmission of TM is for pitch $p_x = p_y \leq 300nm$ larger than TE whereas for $p_x = p_y \geq 300nm$ the reverse occurs. But for the APSM the degree of polarization is less than for the Chromium mask.

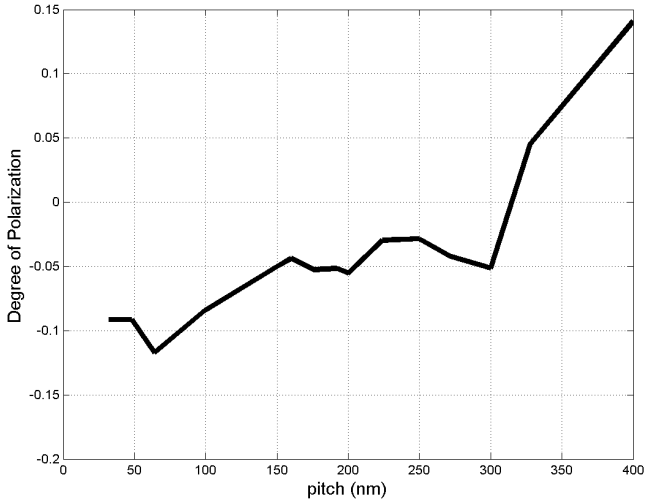

Figure 6. Degree of polarization for binary Chromium mask with thickness 70nm. The illumination is off-axis. 0th order results forλ = 193nm.

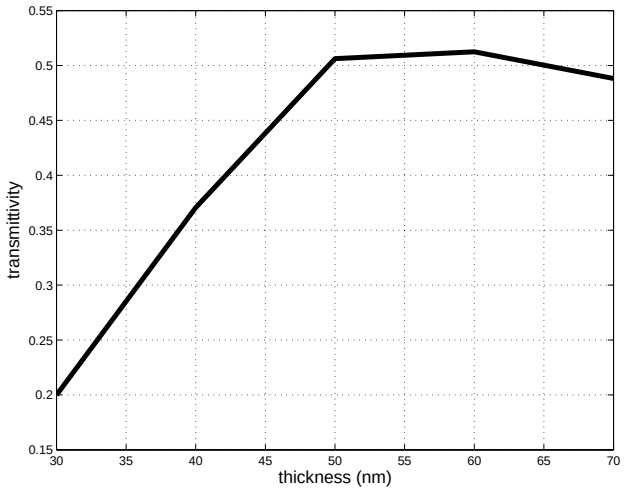

Figure 7. Transmittivity for binary Chromium mask with pitch 70nm. The illumination is on-axis. 0th order results for λ =193nm.

Finally to give an indication of results obtained in the case of topography, we consider some aerial images for the case of the Chromium masks. The field in the image plane of the lens with NA=0.91 is obtained by coherently adding the complex amplitudes of the transmitted orders that are captured by the lens. The aerial image is then the squared modular of the image field.

In Fig. 9 we compare masks (a), (b) and (c) of Fig. 3. The illumination is on-axis, the thickness of the chromium is 70nm and the pitch is 400nm. It is seen that the spots are smaller in the x-direction for the case of a mask with serifs. We get even a better image for the case of a mask with bars. In Fig. 10 the aerial images of the same masks are shown but now for off-axis TM polarized illumination. Now the use of serifs and bars does not give a noticeable improvement, even could have a detrimental impact on image contrast. In Fig. 11 the incident polarization is TE and in that case the images for the mask with serifs and bars are considerably better than the mask of square shape.

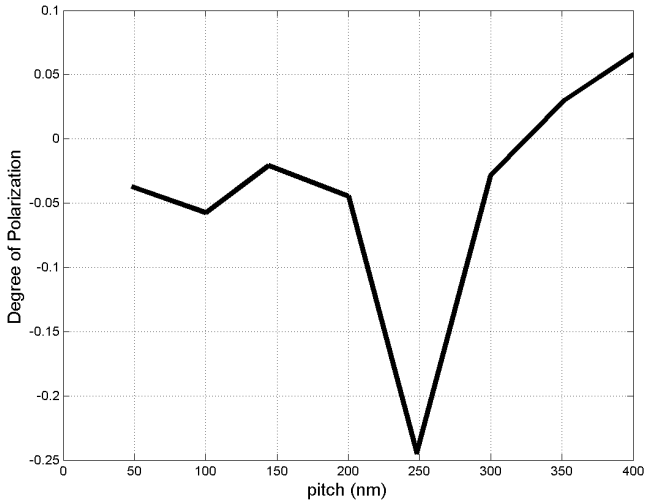

Figure 8. Degree of polarization for PSM mask with thickness 70nm. The illumination is off-axis. 0th order results for$\lambda = 193$nm.

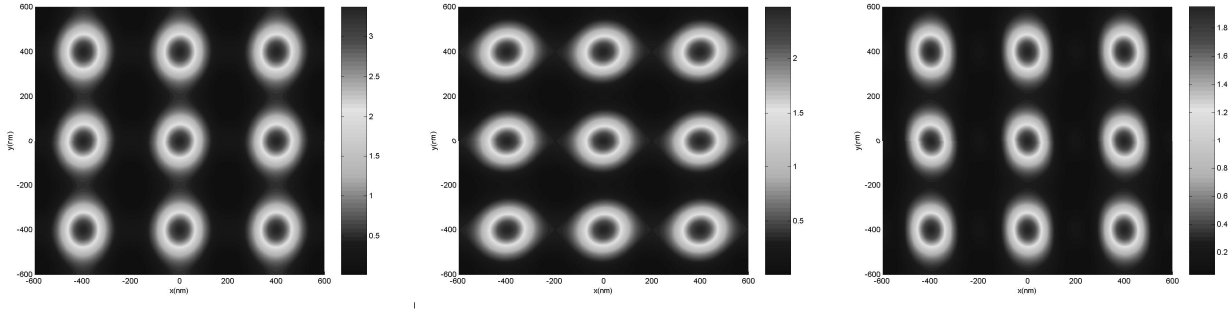

Figure 9. Aerial image for binary Chromium mask with pitch 400nm and thickness of the Chromium of 70nm. The illumination is on-axis. The aerial images for the Chromium mask (a), (b) and (c) in Fig. 3 are shown at the left, in the middle and at the right, respectively.

4. CONCLUSION

A finite element model for the rigorous calculation of the electromagnetic diffraction by periodic 3D photo masks has described.

The model has been applied to binary Chromium masks and to attenuated phase shifting masks we studied the influence of pitch, layer thickness and the polarization of the illumination on the transmission by the mask and on the aerial image. Considerable differences between two orthogonal polarization were found.

ACKNOWLEDGMENTS

The authors would like to thank the Dutch Ministry of Economic Affairs for providing financial support during this research under the project BTS01044.

REFERENCES

1. Andrew Estroff, "Mask induced polarization ," Proc. SPIE 5377, (2004).
2. J. P. Berenger, "A perfectly matched layer for the absorption of electromagnetic waves", J. Comput. Phys. **114**, 185-200 (1994).
3. J. Nédélec,"Mixed finite elements in $\mathbf{R}^3$", Numer. Math. **35**, 315-341 (1980).

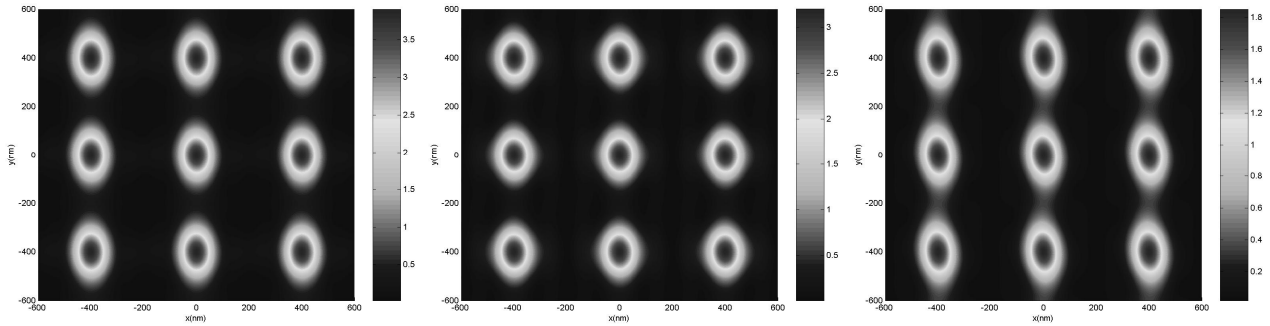

Figure 10. Aerial image for binary Chromium mask with pitch 400nm and thickness of the Chromium of 70nm. The illumination is off-axis and TM polarized. The aerial images for the Chromium mask (a), (b) and (c) in Fig. 3 are shown at the left, in the middle and at the right, respectively.

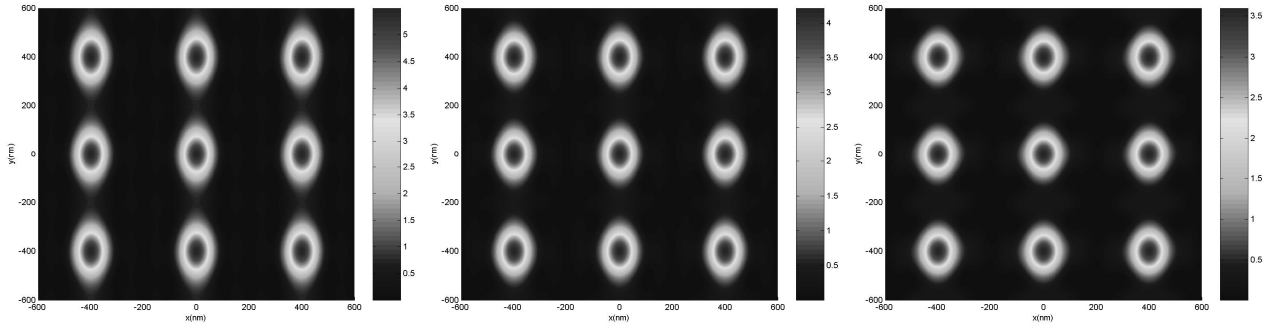

Figure 11. Aerial image for binary Chromium mask with pitch 400nm and thickness of the Chromium of 70nm. The illumination is off-axis and TE polarized. The aerial images for the Chromium mask (a), (b) and (c) in Fig. 3 are shown at the left, in the middle and at the right, respectively.